Inorganic Chemistry

Article

pubs.acs.org/IC

Crystal Structure, Physical Properties, and Electronic and Magnetic Structure of the Spin $S = {}^5/_2$ Zigzag Chain Compound $Bi_2Fe(SeO_3)_2OCl_3$

Peter S. Berdonosov,*[,†] Elena S. Kuznetsova,[†] Valery A. Dolgikh,[†] Alexei V. Sobolev,[†] Igor A. Presniakov,[†] Andrei V. Olenev,[‡,§] Badiur Rahaman,[§] Tanusri Saha-Dasgupta,[§] Konstantin V. Zakharov,[∥] Elena A. Zvereva,[∥] Olga S. Volkova,[∥,⊥] and Alexander N. Vasiliev[∥,⊥,#]

[†]Faculty of Chemistry, Lomonosov Moscow State University, Moscow 119991, Russia

[‡]Department of Chemistry, University of California, Davis, California 95616, United States

[§]S. N. Bose National Centre for Basic Sciences, Kolkata 700098, India

[∥]Faculty of Physics, Lomonosov Moscow State University, Moscow 119991, Russia

[⊥]Theoretical Physics and Applied Mathematics Department, Ural Federal University, Ekaterinburg 620002, Russia

[#]National University of Science and Technology "MISiS", Moscow 119049, Russia

Supporting Information

ABSTRACT: We report the synthesis and characterization of the new bismuth iron selenite oxochloride $Bi_2Fe(SeO_3)_2OCl_3$. The main feature of its crystal structure is the presence of a reasonably isolated set of spin $S = {}^5/_2$ zigzag chains of corner-sharing FeO_6 octahedra decorated with BiO_4Cl_3, BiO_3Cl_3, and SeO_3 groups. When the temperature is lowered, the magnetization passes through a broad maximum at $T_{max} \approx 130$ K, which indicates the formation of a magnetic short-range correlation regime. The same behavior is demonstrated by the integral electron spin resonance intensity. The absorption is characterized by the isotropic effective factor $g \approx 2$ typical for high-spin Fe^{3+} ions. The broadening of ESR absorption lines at low temperatures with the critical exponent $\beta = {}^7/_4$ is consistent with the divergence of the temperature-dependent correlation length expected for the quasi-one-dimensional antiferromagnetic spin chain upon approaching the long-range ordering transition from above. At $T_N = 13$ K, $Bi_2Fe(SeO_3)_2OCl_3$ exhibits a transition into an antiferromagnetically ordered state, evidenced in the magnetization, specific heat, and Mössbauer spectra. At $T < T_N$, the ^{57}Fe Mössbauer spectra reveal a low saturated value of the hyperfine field $H_{hf} \approx 44$ T, which indicates a quantum spin reduction of spin-only magnetic moment $\Delta S/S \approx 20\%$. The determination of exchange interaction parameters using first-principles calculations validates the quasi-one-dimensional nature of magnetism in this compound.

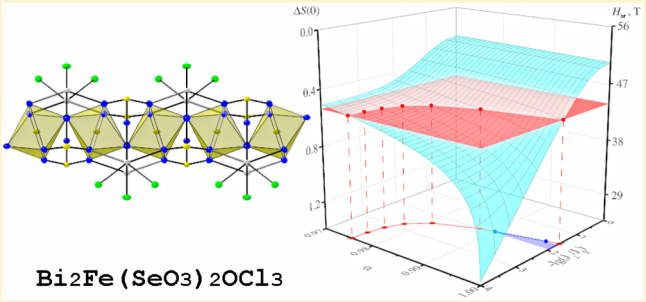

INTRODUCTION

Magnetism in quasi-one-dimensional magnetic systems, which are quantum in nature, is currently a hot topic due to the diversity of exciting physical phenomena exhibited by them. To mention a few, we note the observation of the spin-Peierls transition in $CuGeO_3$,[1] the charge-driven and orbital-driven spin-Peierls-like transitions in NaV_2O_5[2] and $NaTiSi_2O_6$,[3] the Bose−Einstein condensation of magnons in $TlCuCl_3$,[4] and the spiral spin structures in $LiCuVO_4$[5,6] and $LiCu_2O_2$.[7−9] All of these compounds are based on ions with a low spin value, i.e. $S = {}^1/_2$, where the quantum effects on physical properties are most pronounced.

Less studied are classical quasi-one-dimensional magnetic systems based on ions with high spin values: e.g., $S = {}^5/_2$. The low-dimensional behavior in classical magnetic systems was found in particular in $FeOHSO_4$,[10] $N_2H_6FeF_5$,[11] and $SrMn_2V_2O_8$;[12] however, no evidence of reduced dimensionality was seen in the sawtooth chain $Rb_2Fe_2O(AsO_4)_2$.[13] All of these compounds undergo three-dimensional ordering at low temperatures resulting from the interchain coupling. The more isolated the chains in a given compound, the more pronounced the quantum aspect in properties is expected to be. In the case of the $S = {}^5/_2$ compound $Mn_2(OD)_2(C_4O_4)$, inelastic neutron scattering measurements have revealed the characteristic behavior of a spin liquid coexisting with a valence bond solid. The departure from classical behavior observed in the high-spin systems is generally assumed to originate from low dimensionality and geometrical frustration.[14]

Compounds with magnetic ions distributed in low-dimensional or layered structures are promising objects for observing such effects. It is well-known that compounds containing

Received: March 26, 2014
Published: May 13, 2014

   dx.doi.org/10.1021/ic500706f | Inorg. Chem. 2014, 53, 5830−5838

elements with lone electron pair ions (I^{5+}, Se^{4+}, Te^{4+}, As^{3+}, Sb^{3+}, Bi^{3+}, Pb^{2+}, etc.) enhance the possibility to form low-dimensional structures.[15] The introduction of halide ions as spacers into selenite(IV) or tellurite(IV) may increase the trend to form low-dimensional crystal structure. Up to now, there have been many prepared and characterized selenite and tellurite halides. The most explored systems contain Cu^{2+} and Ni^{2+}, due to the interest in spin $^1/_2$ or 1 lattices or to the formation of different coupling regimes.[16] Systems with much higher spin states have not yet been explored. Only $Cr_3Te_5O_{13}Cl_3$,[17] $Fe_6Ca_2(SeO_3)_9Cl_4$,[18] and Fe^{3+} tellurite halides[19] are known up to now. To the best of our knowledge, $Fe_6Ca_2(SeO_3)_9Cl_4$ is the only known selenite halide that contains Fe(III) ions. When this work was considered for publication, the new iron selenite fluoride $FeSeO_3F$ was described.[19e] In the crystal structure of this compound *cis*-$[FeO_4F_2]$ octahedra form Heisenberg antiferromagnetic chains.[19e]

In the present study, we report the synthesis and crystal structure determination of a new quasi-one-dimensional compound, the bismuth iron selenite oxochloride $Bi_2Fe(SeO_3)_2OCl_3$, and its characterization through magnetization, specific heat, electron spin resonance, and ^{57}Fe Mössbauer spectroscopy measurements. Significant quantum reduction of the spin-only value of the iron magnetic moment is found through the analysis of the low-temperature Mössbauer spectra. The electronic and magnetic structures of $Bi_2Fe(SeO_3)_2OCl_3$ have been obtained through first-principles calculations. The calculated parameters of nearest-neighbor intrachain $J_{\parallel}$ and next-nearest-neighbor intrachain $J_{\parallel}'$ exchange interactions, as well as interchain $J_{\perp}$ exchange interactions, agree with experimental data, supporting the quasi-one-dimensional nature of the compound.

EXPERIMENTAL DETAILS

Originally single crystals of the new compound were found in the reaction mixture of chemically pure BiOCl (0.2341 g, 0.899 mmol), FeOCl (0.098 g, 0.913 mmol) and anhydrous SeO_2 (0.202 g, 1.82 mmol) which was heated in a sealed quartz tube to 300 °C for 168 h. FeOCl was obtained from a mixture of Fe_2O_3 (1.3457 g , 8.427 mmol) and anhydrous $FeCl_3$ (1.3620 g, 8.397 mmol) in a sealed, evacuated quartz tube at 370 °C for 48 h similarly to the procedure in ref 20.

After a structure determination the composition of the compound was confirmed by directed synthesis from a mixture of chemically pure Bi_2O_3 (0.4792 g, 1.028 mmol), SeO_2 (0.229 g, 2.064 mmol), and $FeCl_3$ (0.165 g, 1.017 mmol) at 300 °C for 60 h according to the reaction

$$Bi_2O_3 + 2SeO_2 + FeCl_3 = Bi_2Fe(SeO_3)_2OCl_3$$

The powder XRD pattern was indexed in the monoclinic space group $P2_1/m$ with cell constants a = 8.575(5) Å, b = 7.133(4) Å, c = 8.603(6) Å, and β = 107.04(3)°. These values are in good agreement with single-crystal experimental results.

We have tried to prepare the bromide analogue of $Bi_2Fe(SeO_3)_2OCl_3$ by the same technique. All our attempts to do this were unsuccessful.

The single crystal selected for the structure determination was analyzed on a KAPPA APEX II diffractometer equipped with a CCD detector. The data set was recorded as ω scans at 0.3° step width and integrated with the Bruker SAINT software package.[21] The data set was indexed in the monoclinic primitive unit cell. The absorption correction was based on fitting a function to the empirical transmission surface as sampled by multiple equivalent measurements (SADABS).[22] The solution and refinement of the crystal structure were carried out using the SHELX suite of programs.[23] It was solved in the space group $P2_1/m$ (No. 11), and the final refinement was performed with anisotropic atomic displacement parameters for all atoms. The pertinent information related to unit cell parameters, data collection, and refinement is provided in Table 1. Selected bond distances are given in Table 2.

Table 1. Data Collection and Structure Refinement Parameters for $Bi_2Fe(SeO_3)_2OCl_3$

composition	$Bi_2Fe(SeO_3)_2OCl_3$
cryst syst	monoclinic
space group	$P2_1/m$ (No. 11)
unit cell dimens	
a, Å	8.570 (2)
b, Å	7.137(2)
c, Å	8.604(2)
β, deg	107.090(3)
V, Å^3	503.1(2)
Z	2
calcd density, g/cm^3	5.612
abs coeff, mm^{-1}	44.355
temp, K	90(2)
wavelength, Å	0.710 73
θ range for data collection, deg	2.48—27.31
no. of rflns collected	5393
no. of unique rflns	1214
no. of params refined	78
R1, wR2 ($I > 2\sigma(I)$)	0.0381, 0.0817
R1, wR2 (all data)	0.0540, 0.0889
largest diff peak and hole, e/Å^3	3.111 and −3.543
goodness of fit on F^2	0.999

Table 2. Bond Lengths (Å) for $Bi_2Fe(SeO_3)_2OCl_3$

bond	distance	bond	distance
Bi1−O3	2.21(1)	Bi2−O3	2.70(1)
Bi1−O4	2.25(1)	Se1−O5	1.67(1)
Bi1−O1 (×2)	2.384(8)	Se1−O1 (×2)	1.751(8)
Bi1−Cl1	2.869(4)	Se2−O4	1.68(1)
Bi1−Cl2 (×2)	3.237(4)	Se2−O2 (×2)	1.718(8)
Bi2−O5	2.43(1)	Fe−O3 (×2)	1.980(5)
Bi2−O2 (×2)	2.539(8)	Fe−O2 (×2)	2.020(8)
Bi2−Cl1 (×2)	2.589(4)	Fe−O1 (×2)	2.041(8)
Bi2−Cl2	2.685(3)		

Thermal decomposition of $Bi_2Fe(SeO_3)_2OCl_3$ was studied on a NETZSCH STA 409 PC instrument under an argon atmosphere. Samples (approximately 16 mg) were heated in an alumina crucible from room temperature up to 1000 °C at a rate of 10 °C/min. The resulting graph is presented in Figure S1 (Supporting Information).

The electron spin resonance (ESR) study was carried out using using a CMS 8400 (ADANI) X-band ESR spectrometer (frequency ∼9.4 GHz, $B \leq 0.7$ T) equipped with a low-temperature mount, operating in the range 6−470 K. The effective g factor of the powder sample of $Bi_2Fe(SeO_3)_2OCl_3$ was calculated with respect to the external reference for the resonance field using BDPA (α,γ-bis(diphenylene)-β-phenylallyl) as a reference material (g_{et} = 2.00359).

The thermodynamic properties of the $Bi_2Fe(SeO_3)_2OCl_3$ ceramic sample, i.e. magnetization and specific heat, were measured with a Quantum Design PPMS-9T Physical Property Measurement System.

The ^{57}Fe Mössbauer spectra were recorded in the temperature range 4.6−300 K using a conventional constant-acceleration spectrometer. The radiation source, ^{57}Co(Rh), was kept at room temperature. All isomer shifts refer to α-Fe at 300 K. The experimental spectra were processed and analyzed using methods of spectral simulation implemented in the SpectrRelax program.[24]

dx.doi.org/10.1021/ic500706f | Inorg. Chem. 2014, 53, 5830−5838

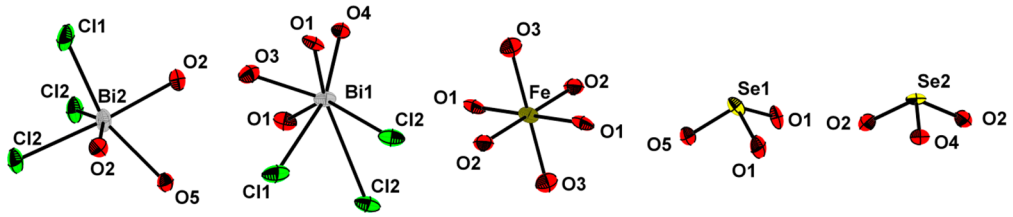

Figure 1. Coordination surroundings of Bi(1), Bi(2), and Fe atoms in the crystal structure of $Bi_2Fe(SeO_3)_2OCl_3$.

First-principles calculations on a plane wave basis, as implemented in VASP,[25] were used to arrive at a self-consistent description of the electronic structure of $Bi_2Fe(SeO_3)_2OCl_3$ within the framework of density functional theory (DFT). The exchange-correlation functional was chosen to be that of the generalized gradient approximation (GGA).[26]

RESULTS AND DISCUSSION

Crystal Structure. In $Bi_2Fe(SeO_3)_2OCl_3$, the bismuth atoms have mixed oxygen and chlorine surroundings (Figure 1). The bond valence sum (BVS) calculation[27] with R_0 and B parameters taken from ref 28 according to the formula

$$\mathrm{BVS} = \sum_i \exp((R_0 - R_i)/B)$$

leads to 2.64 for Bi1 atoms in case of a strongly asymmetric BiO_4Cl polyhedron. The addition of two Bi1−Cl2 bonds with lengths of more than 3 Å increases this value to 2.90. Therefore, the coordination surroundings for Bi1 atoms may be represented as the seven-vertex polyhedron $Bi1O_4Cl_3$. The lone pair activity of the Bi1 atom may be the reason for such asymmetrical surroundings. Bi2 atoms have six nearest neighbors: i.e., three oxygen atoms at distances of 2.42−2.54 Å and three chlorine atoms at distances of 2.58−2.68 Å. The BVS value for this polyhedron is 3.07. The polyhedron for the Bi2 atom is a distorted $Bi2O_3Cl_3$ octahedron with the Bi2 atom situated in the plane formed by two O2 and two Cl2 atoms (Figure 1, Table 2). Fe(III) atoms are surrounded by six oxygen atoms in the FeO_6 octahedron with bond lengths in the range 1.98−2.04 Å (Figure 1, Table 2). The BVS value for this polyhedron is 3.02. Selenium atoms are surrounded by oxygen atoms only and form SeO_3 groups with the pyramidal shape SeO_3E, where E is the lone pair of Se(IV). Se−O distances are in the usual range: 1.67−1.75 Å (Table 2) (see for example refs 16 and 18). The BVS values are 3.84 and 4.02 for Se1 and Se2, respectively.

FeO_6 octahedrons are connected into zigzag chains by common O3 vertexes. FeO_6 octahedrons share O1−O3 edges with the $Bi1O_4Cl_3$ polyhedron and O2 vertexes with the $Bi2O_3Cl_3$ polyhedron. These Bi polyhedrons are connected by common Cl1 and Cl2 vertexes. FeO_6 octahedrons share O2 and O1 vertexes with $Se1O_3$ and $Se2O_3$ groups. The third oxygen atoms of Se1 and Se2 groups, i.e. O4 and O5, are shared with Bi1 and Bi2 polyhedrons. Therefore, SeO_3 groups additionally stitch Fe−Bi−O chains. A polyhedral representation of the $Bi_2Fe(SeO_3)_2OCl_3$ crystal structure is shown in Figure 2. According to this description, the crystal structure of $Bi_2Fe(SeO_3)_2OCl_3$ can be considered as layered. The FeO_6 octahedron chains running along the b axis form layers perpendicular to the c axis. The distance between Fe atoms in the chain is 3.569(1) Å, whereas the distances between Fe atoms from different chains are 8.570(2) and 8.604(2) Å. On the basis of this fact the magnetic sublattice may be suggested as being quasi-one-dimensional.

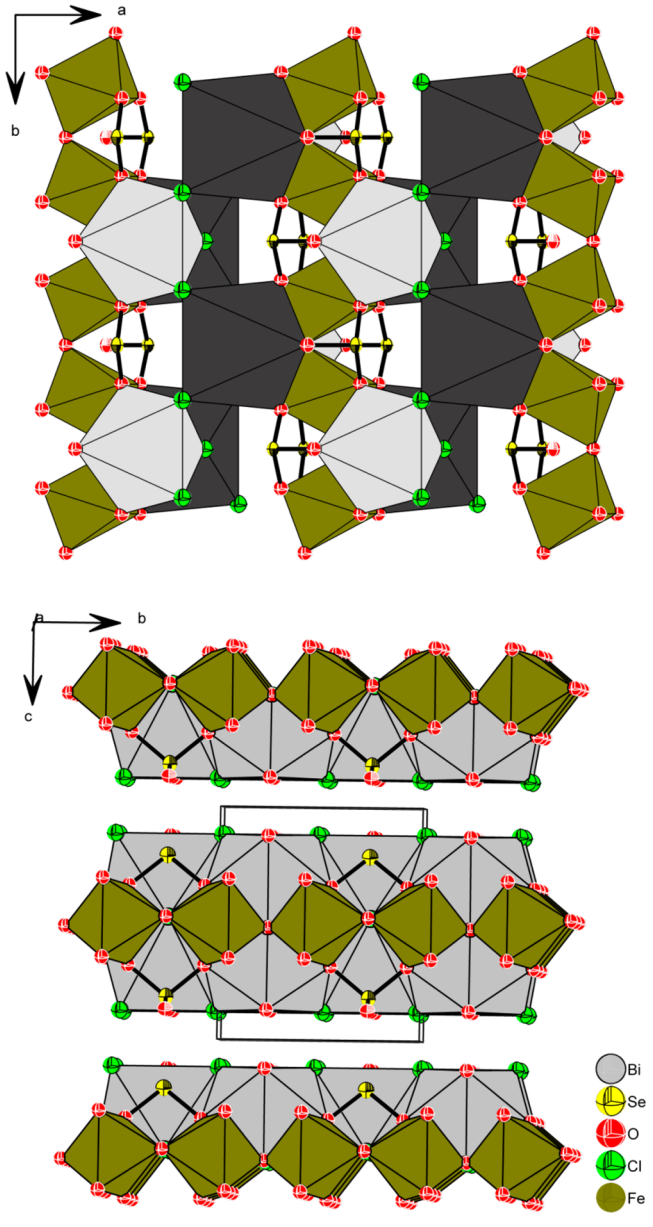

Figure 2. Polyhedrons of Bi1, Bi2, and Fe atoms in the crystal structure of $Bi_2Fe(SeO_3)_2OCl_3$ (upper panel). Polyhedral representation of Fe−Bi−O−Cl layer along the c axis (upper panel) and a axis (lower panel). Bi1 polyhedrons are drawn as dark and Bi2 polyhedrons as light. SeO_3 groups stitch FeO_6 and BiO_4Cl_3 polyhedrons.

Thermal Stability Study. As follows from our experiment $Bi_2Fe(SeO_3)_2OCl_3$ is stable up to 400 °C. At higher temperatures, decomposition begins within at least four steps

dx.doi.org/10.1021/ic500706f | Inorg. Chem. 2014, 53, 5830−5838

with DSC peaks at 440, 500, 825, and 915 °C. The weight loss does not end at 1000 °C and amounts to a total of about 60% from the starting amount of the substance. It is possible to suggest that the first step of decomposition with an illegible plateau in the range 440−500 °C corresponds to loss of a $SeOCl_2$ molecule. The observed weight loss of about 20% is in good agreement with the calculated value, 19.6%. The plateau in the 500−750 °C temperature range may be attributed to loss of all chlorine atoms and two molecules of SeO_2 (observed 41%, calculated 38.7%).

Electron Spin Resonance. The evolution of the X-band ESR spectra with temperature for a powder sample of $Bi_2Fe(SeO_3)_2OCl_3$ is shown in Figure 3. A qualitative analysis

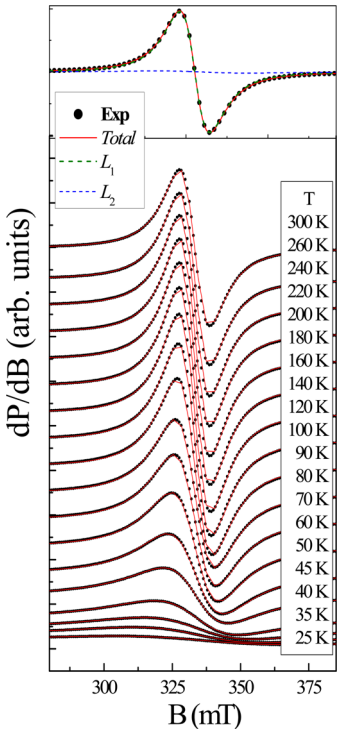

Figure 3. Temperature evolution of the first-derivative ESR absorption line for a powder sample of $Bi_2Fe(SeO_3)_2OCl_3$: (black points) experimental data; (solid lines) fitting by the sum of two Lorentzians (eq 1). The top panel represents an example of the spectrum decomposition along with two resolved lines at room temperature.

of the line shape was performed, taking into account two circular components of the exciting linearly polarized microwave field by fitting of the experimental spectra in accordance with the sum of two Lorentzian functions in the form

$$\frac{dP}{dB} \propto \frac{d}{dB}\left[\frac{\Delta B}{\Delta B^2 + (B - B_r)^2} + \frac{\Delta B}{\Delta B^2 + (B + B_r)^2}\right] \quad (1)$$

This formula describes a symmetric line, where P is the power absorbed in the ESR experiment, B is the magnetic field, B_r is the resonance field, and ΔB is the the line width. It was found that a proper description of the ESR spectra requires including the two spectral components L_1 and L_2. The upper panel in Figure 3 represents an example of the spectrum decomposition along with the two resolved lines L_1 and L_2 at room temperature. Obviously, the line L_1 appears to introduce the main contribution to the absorption signal and is at least 2 orders of magnitude more intense than the additional weak line L_2. One can assume that the line L_1 originates presumably from a quasi-one-dimensional subsystem of Fe^{3+} ions, while the latter line L_2 possibly refers to a small amount of paramagnetic defects or impurities. The results of ESR line shape fitting in accordance with eq 1 are shown by solid lines in Figure 3. Apparently, the fitted curves are in good agreement with the experimental data over the whole temperature range studied.

The main resonance line L_1 is characterized by the effective g factor $g = 1.999 \pm 0.005$, which is typical of S-type Fe^{3+} ions in octahedral coordination (Figure 4). The quasi-one-dimensional

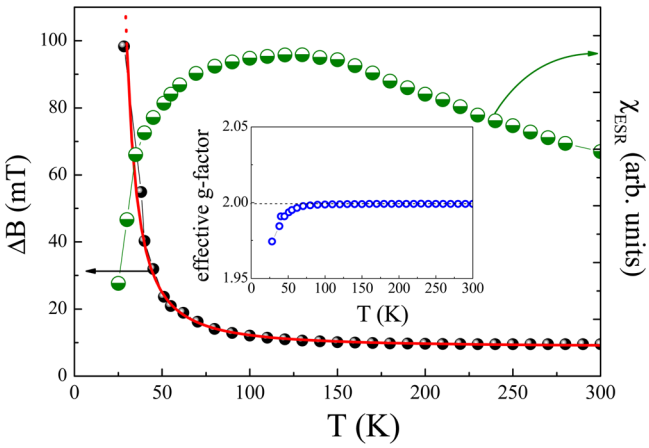

Figure 4. Temperature dependence of the effective g factor, the ESR line width ΔB, and the integral ESR intensity χ_{ESR} for $Bi_2Fe(SeO_3)_2OCl_3$ derived from fitting of ESR spectra in accordance with eq 1 for the main resonance mode L_1 related to the signal from a quasi-one-dimensional chain of Fe^{3+} cations. The red solid line is the fit according to eq 2.

behavior of the ESR signal in $Bi_2Fe(SeO_3)_2OCl_3$ is clearly seen in the temperature dependence of the ESR integral intensity χ_{ESR} of the L_1 line, which is proportional to the number of magnetic spins and was estimated by double-integration of the first-derivative ESR spectra (Figure 4). Similarly to the static magnetic susceptibility (as shown below) this value passes through a broad maximum at about $T_{max} \approx 130$ K. The line width of this component, ΔB, increases progressively at decreasing temperature, and a pronounced degradation of the ESR absorption line occurs at low temperature (Figure 3). This low-T signal fading could be due to a shortening of spin−spin correlations as the temperature approaches the Néel temperature T_N from above.

Anomalous broadening of the line upon approaching the long-range ordering transition from above has been observed earlier for a wide class of antiferromagnetic, spin-glass, diluted magnetic, and lower dimensional systems[29] including a great number of antiferromagnetic compounds with trivalent iron.[30] It has been treated as critical behavior due to the slowing down of spin fluctuations on approaching the critical temperature. This causes the divergence of the spin correlation length, which in turn affects the spin−spin relaxation time, resulting in broadening of the ESR line. According to Huber's formula,[31] which evolved from the theory of Mori and Kawasaki,[32,33] the ESR line width varies with temperature near the Néel point in accordance with[34]

dx.doi.org/10.1021/ic500706f | Inorg. Chem. 2014, 53, 5830−5838

$$\Delta B(T) = \Delta B^{*} + A\left[\frac{T_N^{ESR}}{T - T_N^{ESR}}\right]^{\beta} \quad (2)$$

where ΔB denotes the ESR line width, A is an empirical parameter, ΔB^{*} is the limiting minimum value of the narrowed line width, which is temperature independent, while the second term reflects the critical behavior with T_N^{ESR} being the temperature of the order−disorder transition and β the critical exponent. In Figure 4, the solid red line superimposed on experimental data represents a least-squares fit of experimental data for the main absorption line according to eq 2. Apparently, this formula remains valid for $Bi_2Fe(SeO_3)_2OCl_3$ in a wide temperature range: 35−300 K. The best fit of the X-band ESR experimental data according to eq 2 resulted in the values $\Delta B^{*} = 10 \pm 1$ mT, $A = 42 \pm 1$ mT, $T_N^{ESR} = 13 \pm 2$ K, and $\beta = 1.75 \pm 0.05$. In the frame of the Kawasaki approach, the critical exponent can be expressed as $\beta = -[{}^1/_2(7 + \eta)\nu - 2(1 - \alpha)]$, where ν describes the divergence of correlation length, η is the critical exponent for the divergence of static correlations, and α relates to divergence of the specific heat, respectively. Using the values $\eta = \alpha = 0$ and $\nu = {}^2/_3$ for a three-dimensional (3D) Heisenberg antiferromagnet,[32] β becomes equal to ${}^1/_3$, which is essentially lower than the experimental value. In case of magnetic systems with lower dimensionality the critical exponent is expressed as $\beta = -(3 - 2\eta)\nu$ and $\beta = -(3.5 - 2\eta)\nu$ for two-dimensional (2D) and one-dimensional (1D) systems, respectively.[35,36] The corresponding values β using the values $\eta = 0$ and $\nu = {}^1/_2$ result in $\beta = {}^3/_2$ and $\beta = {}^7/_4$ for 2D and 1D systems, respectively. Obviously, the latter value is in good agreement with the experimentally observed value.

Thermodynamics. The temperature dependence of magnetic susceptibility χ of $Bi_2Fe(SeO_3)_2OCl_3$ taken in the field-cooled regime at $B = 0.1$ T is shown in Figure 5. At

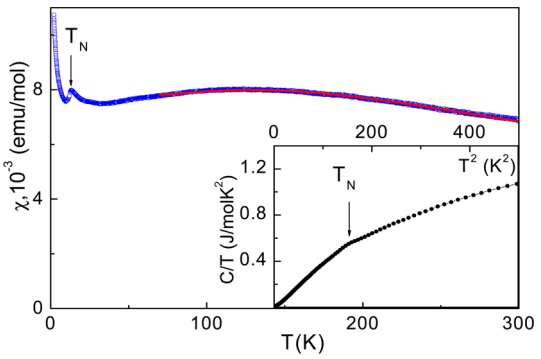

Figure 5. Temperature dependence of magnetic susceptibility in $Bi_2Fe(SeO_3)_2OCl_3$. The solid line represents the fit in a Heisenberg $S = \infty$ antiferromagnetic chain model. The inset represents the temperature dependence of specific heat on the C/T vs T^2 scale.

elevated temperatures, the field-cooled and zero-field-cooled curves coincide but slightly deviate from each other at low temperatures. This divergence is ascribed routinely to defects and/or impurities; we neglect it in further discussion. However, the increase of magnetic susceptibility at the lowest temperatures could be of intrinsic origin. In zigzag chains of FeO_6 octahedra the Dzyaloshinskii−Moriya interaction results in canting of magnetic moments, seen as the rise of magnetic susceptibility at low temperatures.[37] On cooling, the magnetic susceptibility passes through a broad maximum at about $T_{max} \approx 130$ K. Well below this maximum, χ demonstrates a Curie-like upturn interrupted by a sharp anomaly at $T_N = 13$ K. This anomaly is seen also in specific heat, as shown in the inset to Figure 5, despite the fact that it is rather weak. Overall, the temperature dependence of χ in $Bi_2Fe(SeO_3)_2OCl_3$ can be treated as formation of the short-range correlation regime at elevated temperatures with subsequent three-dimensional long-range order at the Néel temperature. Note that T_{max} and T_N differ by 1 order of magnitude, signifying the quasi-low-dimensional nature of magnetism in $Bi_2Fe(SeO_3)_2OCl_3$.

In accordance with the structural features of $Bi_2Fe(SeO_3)_2OCl_3$, the dominant magnetic exchange interaction $J_{\parallel}$ in this compound is realized within the chains of corner-sharing FeO_6 octahedrons. The interaction through apical oxygen atoms is assumed to be antiferromagnetic for both 90 and 180° angles of $Fe^{3+}-O^{2-}-Fe^{3+}$ bonds.[38] Thus, quasi-isolated antiferromagnetic $S = {}^5/_2$ chains define the magnetic behavior of $Bi_2Fe(SeO_3)_2OCl_3$ at high temperatures: i.e., produce the correlation maximum in $\chi(T)$ dependence. The calculations of thermodynamic properties of the Heisenberg $S = {}^5/_2$ antiferromagnetic chain define the ratio for the value of magnetic susceptibility in the maximum χ_{max}, its temperature $T(\chi_{max})$,and g factor through the expression[39]

$$\frac{\chi_{max}[T(\chi_{max})]}{g^2} = 0.38 \quad (3)$$

In $Bi_2Fe(SeO_3)_2OCl_3$, this quantity is only 0.26. This low value indicates either reduction of the spin-only magnetic moments of the iron atoms or frustration of the dominant nearest-neighbor exchange interaction within the chains.

In the simplified model of unique nearest-neighbor exchange interaction, the position of the maximum of magnetic susceptibility defines the exchange interaction parameter $J_{\parallel}$ through the expression

$$\frac{k_B[T(\chi_{max})]}{|J_{\parallel}|} = 10.6 \quad (4)$$

The estimation of antiferromagnetic exchange interaction parameter according to eq 4 gives $J_{\parallel} = 12$ K.

It can be determined more precisely using Fisher's model of $S = \infty$ infinite chains:[39]

$$\chi_{chain} = \frac{N_A g^2 S(S+1)\mu_B^2}{3k_B T}\frac{1+u}{1-u}$$
$$u = \coth\left(\frac{2J_{\parallel}S(+1)}{k_B T}\right) - \frac{k_B T}{2J_{\parallel}S(+1)} \quad (5)$$

where N_A, μ_B, and k_B are Avogadro, Bohr, and Boltzmann constants. As is shown in Figure 5, the $\chi(T)$ dependence can be fitted by the sum of the temperature-independent term χ_0, the Curie−Weiss term related to the defects C/T, and Fisher's magnetic susceptibility of the chain χ_{chain}:

$$\chi = \chi_0 + \frac{C}{T} + \alpha\chi_{chain} \quad (6)$$

Here, the temperature-independent term was estimated from the summation of Pascal's constants of the atoms forming $Bi_2Fe(SeO_3)_2OCl_3$ as $\chi_0 = -2.1 \times 10^{-4}$ emu/mol.[40] The Curie constant $C = 4.7 \times 10^{-2}$ emu K/mol gives an estimation of the impurities/defects concentration ($S = {}^5/_2$) as about 1%. The coefficient $\alpha = 0.92$ highlights the deviation from the one-dimensional model. In this case, the estimation of the

dx.doi.org/10.1021/ic500706f | Inorg. Chem. 2014, 53, 5830−5838

antiferromagnetic intrachain exchange interaction parameter amounts to $J_{\|} \approx 17$ K.

The interchain interaction in $Bi_2Fe(SeO_3)_2OCl_3$, $J_\perp$, can be calculated from the equation[41]

$$\exp\left(\frac{2|J_{\|}|}{kT_N}\right) = \frac{4 + Z\eta}{Z\eta} \quad (7)$$

where $\eta = J_\perp/J_{\|}$ and Z is the number of nearest-neighboring chains ($Z = 4$). This expression gives the estimates $\eta = 0.08$ and $J_\perp \approx 1.4$ K.

^{57}Fe Mössbauer Spectroscopy. The ^{57}Fe Mössbauer spectra of $Bi_2Fe(SeO_3)_2OCl_3$ were recorded both below and above the Néel temperature $T_N = 13$ K. As shown in Figure 6,

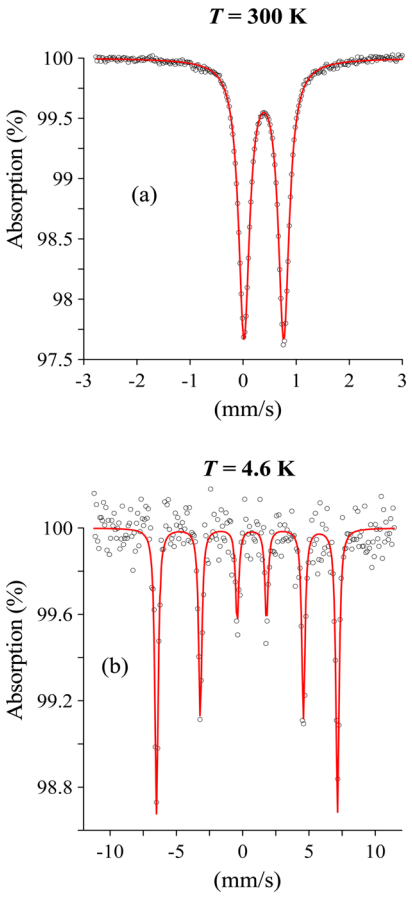

Figure 6. Representative ^{57}Fe Mössbauer spectra of powder−crystal $Bi_2Fe(SeO_3)_2OCl_3$ recorded both above (upper panel) and below (lower panel) the Néel temperature.

the spectrum at room temperature can be fitted by a quadrupole doublet with isomer shift value $\delta_{300\ K} = 0.39 \pm 0.01$ mm/s, which falls in the range for high-spin Fe^{3+} ions in an octahedral oxygen environment.[24] The quadrupole splitting value $\Delta_{300\ K} = 0.20 \pm 0.01$ mm/s is rather high for a 6S electronic state of Fe^{3+} ions. This might be due to the distortion of oxygen octahedrons FeO_6 within the isolated iron chains in the $Bi_2Fe(SeO_3)_2OCl_3$ structure. No visible anomalies in the $\delta(T)$ and $\Delta(T)$ dependences were seen on cooling, thus indicating that there are no structural transitions below room temperature.

In the antiferromagnetic phase ($T = 4.6$ K) the ^{57}Fe Mössbauer spectrum consists of a magnetic Zeeman sextet, as shown in Figure 6. The approximated saturation value of the hyperfine field $H_{hf}(T\rightarrow 0) \approx 44$ T is anomalously low for a high-spin iron atom in octahedral oxygen coordination, for which H_{hf} is usually about 56 T.[42] The spin reduction of about ~20% cannot be accounted for by crystal field or covalency effects and can be attributed only to quantum spin reduction, predicted to be large in quasi-one-dimensional antiferromagnets.[43] The quantum spin reduction is the function of the ratio H_A/H_E (where H_A and H_E are crystal anisotropy and exchange fields, respectively) and of the ratio $\xi = J_\perp/J_{\|}$ of the interchain to intrachain exchange interaction parameters. Following spin-wave theory for an antiferromagnetic systems,[43] the zero-point spin reduction $\Delta S(0) = ({}^5/_2 - \langle S(0)\rangle)$ at each magnetic sublattice can be given by

$$\Delta S(0) = \frac{4abc}{\pi^3}\int_0^{\pi/2a}\int_0^{\pi/2b}\int_0^{\pi/2c}[(1-\alpha\gamma_k^{\ 2})^{-1/2} - 1]\, dk_x\, dk_y\, dk_z \quad (8)$$

where $\alpha = (1 + H_A/H_E)^{-2}$ and γ_k is the structure factor defined by

$$\gamma_k = \frac{\cos\ k_y b + \xi[(\cos\ k_x a + \cos\ k_z c)]}{1 + 2\xi} \quad (9)$$

Here, b is the lattice constant along the iron chains, a and c are the lattice constants perpendicular to the chains, and k_x, k_y, and k_z are the components of the wavevector $\mathbf{k}$ along principal lattice vectors. Spin fluctuations (8) or spin waves are present even at absolute zero temperature. These fluctuations reduce the mean value $\langle S(0)\rangle$ of the Fe^{3+} ions below $S(0) = {}^5/_2$. This reduction is directly measurable from the Mössbauer spectra, since the magnitude of the magnetic hyperfine field H_{hf} is proportional to $\langle S(0)\rangle$. We evaluated numerically the integral (8) for various values of α and ξ. The result of $\Delta S(0)$ evaluation is shown in Figure 7. The values of the hyperfine field $H_{hf}(0)$ corresponding to the spin reduction are indicated on the right-hand scale axis of Figure 7. For $\Delta S(0)$ we assumed a saturation $H_{hf}(0)$ value of 54 T for Fe^{3+} ions in FeO_6 octahedral coordination, corrected for covalence effects.[44]

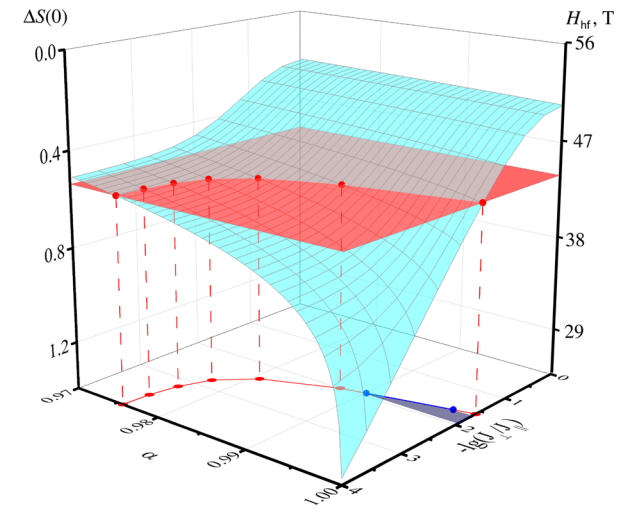

Figure 7. Diagram of calculated zero-point spin reduction $\Delta S(0)$ and corresponding hyperfine field $H_{hf}(0)$ as a function of the anisotropy ratio H_A/H_E and the ratio $\xi = J_\perp/J_{\|}$ of the interchain to intrachain exchange interaction parameters.

dx.doi.org/10.1021/ic500706f | Inorg. Chem. 2014, 53, 5830−5838

According to this figure, the $\Delta S(0)$ value increases rapidly when the magnetic dimensionality ξ and anisotropy H_A/H_E are reduced. Using the usually observed values for $H_A/H_E = (1-5) \times 10^{-3}$,[43] we estimated $\xi \approx 0.01-0.03$. This is in good assumption with the notion that the $Bi_2Fe(SeO_3)_2OCl_3$ compound is a quasi-one-dimensional spin system.

First-Principles Electronic Structure Calculations. The spin-polarized density of states, projected onto Fe d, O p, Cl p, Se p, and Bi p states, are shown in Figure 8. We find that

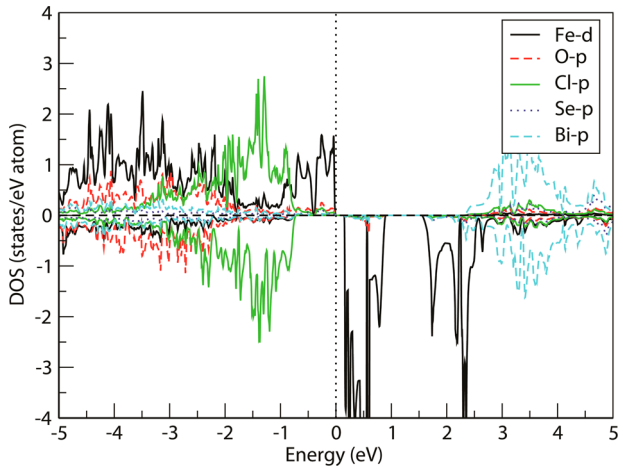

Figure 8. Spin-polarized density of states for $Bi_2Fe(SeO_3)_2OCl_3$ projected onto Fe d, O p, Cl p, Se p, and Bi p states. Zero energy is set at the GGA Fermi energy. The states in majority and minority spin channels are shown as positive and negative values.

octahedral crystal field split Fe t_{2g} and e_g states are completely filled in the majority spin channel and completely empty in the minority spin channel, suggesting the nominal Fe^{3+} or d^5 valence of Fe. Both Bi p and Se p are found to be nearly empty, suggesting the nominal Bi^{3+} and Se^{4+} valences, while the O p and Cl p states are found to be mostly occupied, suggesting the nominal 2− and 1− valence states, respectively. The O p and Cl/Se p states show finite, nonzero hybridization with Fe d states close to the Fermi energy, which contributes to the superexchange path of the magnetic interaction between two Fe sites. The magnetic moment, calculated with the single-electron approximation of DFT, at the Fe site is found to be 4.33 μ_B, with rest of the moment sitting at neighboring O and Cl sites, with a total magnetic moment of 5 μ_B per formula unit.

In order to estimate the various Fe−Fe magnetic exchange interactions present in the compound, the *n*th-order muffin tin orbital (NMTO) based downfolding technique[45] was applied to construct Fe d only Wannier orbitals by downfolding all the degrees of freedom associated with O, Cl, Se, and Bi and keeping active only the Fe d degrees of freedoms. This procedure provides renormalization of Fe d orbitals due to hybridization from O p, Cl p, Se p, and Bi p. The effective Fe−Fe hopping interactions were obtained by the real-space representation of the Hamiltonian in the effective Fe d Wannier function basis. The dominant hopping interactions are found to be the nearest-neighbor intrachain $t_{\parallel}$, next-nearest-neighbor intrachain $t_{\parallel}'$, and interchain $t_{\perp}$. The magnetic exchange interactions, $J_{\parallel}$, $J_{\parallel}'$, and $J_{\perp}$, can be obtained from the knowledge of hopping interactions and the on-site energies of various Fe d states through a superexchange formula,[46] with a choice of the appropriate Hubbard *U* parameter. Such an approach is found to be highly successful in a number of applications.[47] The paths for dominant magnetic interactions are shown in Figure 9. We see that $J_{\parallel}$ is mediated by an Fe−O−Fe superexchange path

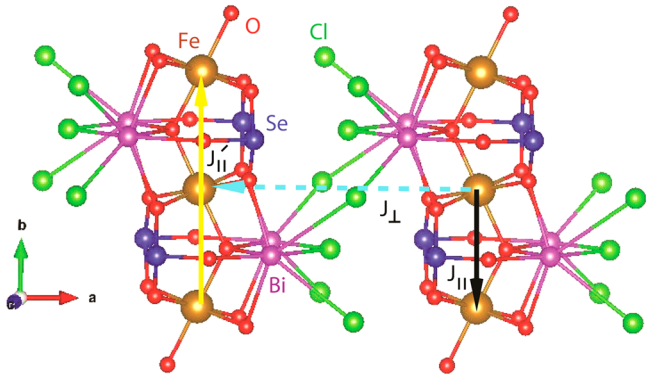

Figure 9. Exchange paths for various magnetic interactions $J_{\parallel}$ (in black), $J_{\parallel}'$ (in cyan), and $J_{\perp}$ (in gold).

where the Fe−O−Fe bond angle is 128.6°, whereas $J_{\parallel}'$ is mediated by a supersuperexchange path, involving Fe, O, Se, and Bi. The interchain interaction $J_{\perp}$ is mediated by a long-range Fe−O−Bi1−Cl−Bi2−O−Fe path. All of the calculated *J* values turned out to be of antiferromagnetic nature, in agreement with the experimental prediction. The *J* values using the superexchange formula, and taking a Hubbard *U* value of 8 eV, turned out to be $J_{\parallel} \approx 21$ K, $J_{\parallel}' \approx 4.6$ K, and $J_{\perp} \approx 0.6$ K, which shows the dominance of the nearest-neighbor intrachain Fe−Fe interaction, proving the quasi-one-dimensional nature of the underlying spin model of the compound. The ratio κ of the next-nearest-neighbor exchange interaction parameter to the nearest-neighbor interaction parameter, $J_{\parallel}'/J_{\parallel} \approx 0.22$, is close to the critical value ($\kappa_{cr} \approx 0.25$) separating the collinear magnetic structures ($\kappa < \kappa_{cr}$) from the helical structures ($\kappa > \kappa_{cr}$).[48] Thus, the magnetic structure in $Bi_2Fe(SeO_3)_2OCl_3$ is expected to be collinear.

CONCLUSIONS

The new bismuth iron selenite oxochloride $Bi_2Fe(SeO_3)_2OCl_3$ was synthesized and its crystal structure determined. The new compound possesses a unique crystal structure with nearly isolated zigzag chains of corner-sharing FeO_6 octahedrons decorated by BiO_4Cl_3 and BiO_3Cl_3 polyhedrons and SeO_3 groups. The physical properties of the new compound are closely related to its crystal structure. At elevated temperatures, the magnetization of the title compound passes through the broad maximum $T_{max} \approx 130$ K, which indicates the formation of a short-range correlation regime and defines the scale of magnetic exchange interactions $J_{\parallel} \approx 17$ K within the chains. The electron spin resonance data corroborate well the static magnetization results and reveal an extended region of short-range order correlations in the compound studied. The critical broadening of ESR absorption lines at low temperatures is consistent with the divergence of temperature-dependent correlation length expected for a quasi-one-dimensional antiferromagnetic spin chain upon approaching the long-range order from above. The ^{57}Fe Mössbauer spectra recorded at $T > T_{max}$ are characteristic for Fe^{3+} ions located in distorted FeO_6 octahedra. At $T = 13$ K, $Bi_2Fe(SeO_3)_2OCl_3$ exhibits a phase transition to the long-range antiferromagnetic state evidenced in specific heat and magnetization measurements. The Mössbauer spectrum at low temperature shows a low

dx.doi.org/10.1021/ic500706f | Inorg. Chem. 2014, 53, 5830−5838

saturated value of the hyperfine field, H_{hf} = 44 T, expected for quasi-one-dimensional systems with a substantial quantum spin reduction $\Delta S/S(0)$ of about 20%. The first-principles calculations, within the framework of density functional theory, allow for estimating both nearest-neighbor $J_{\parallel}$ and next-nearest-neighbor $J_{\parallel}'$ exchange interaction parameters within the chains, as the interchain interaction $J_{\perp}$. These values are found to be in good correspondence with estimates based on the simplified description of magnetism in quasi-one-dimensional systems. For the ratio of intrachain to interchain exchange interaction parameters $\xi = J_{\perp}/J_{\parallel}$ the analysis of ^{57}Fe Mössbauer data and magnetic structure calculations give a value of ∼0.03, significantly lower than that obtained in Fisher's model.[38] This underlines the importance of accounting for additional exchange interactions within the chains. The reduction of the spin-only moments in $Bi_2Fe(SeO_3)_2OCl_3$, which is a *classical* ($S = {}^5/_2$) magnet, is the manifestation of the quantum effects in low dimensionality.

Finally, the practical aspect of the quasi-one-dimensional magnetic systems is the possibility of significant enhancement of thermal conductivity in well-defined directions, i.e. along spin chains[49−51] or spin ladders,[52,53] in basically three-dimensional crystal lattices. This enhancement in quantum spin systems is attributed to the large contribution of magnetic excitations. While the investigation of these phenomena needs single crystals of the title compound, which are not yet available, the present work could be considered as a necessary prerequisite for such a study.

■ ASSOCIATED CONTENT

Supporting Information

CIF file giving crystallographic data for $Bi_2Fe(SeO_3)_2OCl_3$ and a figure giving the results of thermal analysis. This material is available free of charge via the Internet at http://pubs.acs.org.

■ AUTHOR INFORMATION

Corresponding Author

*P.S.B.: e-mail, berdonosov@inorg.chem.msu.ru; tel, +7(495) 939-3504; fax, +7(495)939-0998.

Present Address

[$]Sine Theta LTD, Moscow 119991, Russia.

Author Contributions

The manuscript was written through contributions of all authors. All authors have given approval to the final version of the manuscript

Notes

The authors declare no competing financial interest.

■ ACKNOWLEDGMENTS

We are grateful to Prof. K. Kovnir (UC Davis) for his help with the structural experiment arrangement and to Prof. V.S. Rusakov (Lomonosov Moscow State University) for MS spectrum measuring at 4.6 K. This work was supported in part from the Ministry of Education and Science of the Russian Federation in the framework of Increase Competitiveness Program of NUST "MISiS" (No. K2-2014-036), by Russian Foundation for Basic Research grants 12-03-00665, 13-02-00174, 14-02-00245, and 14-02-92693 and by the President of Russia grant MK-7138.2013.2.

■ REFERENCES

(1) Hase, M.; Terasaki, I.; Uchinokura, K. *Phys. Rev. Lett.* **1993**, *70*, 3651−3654.
(2) Isobe, M.; Ueda, Y. *J. Phys. Soc. Jpn.* **1996**, *65*, 1178−1181.
(3) Ninomiya, E.; Isobe, M.; Vasil'ev, A. N.; Ueda, Y. *J. Phys. Soc. Jpn.* **2002**, *71*, 1423−1426.
(4) Nikuni, T.; Oshikawa, M.; Oosawa, A.; Tanaka, H. *Phys. Rev. Lett.* **2000**, *84*, 5868−5871.
(5) Vasil'ev, A. N.; Ponomarenko, L. A.; Manaka, H.; Yamada, I.; Isobe, M.; Ueda, Y. *Phys. Rev. B* **2001**, *64*, 024419.
(6) Enderle, M.; Mukherjee, C.; Fåk, B.; Kremer, R. K.; Broto, J.-M.; Rosner, H.; Drechsler, S.-L.; Richter, J.; Malek, J.; Prokofiev, A.; Assmus, W.; Pujol, S.; Raggazzoni, J.-L.; Rakoto, H.; Rheinstädter, M.; Rønnow, H. M. *Europhys. Lett.* **2005**, *70*, 237−243.
(7) Gippius, A. A.; Morozova, E. N.; Moskvin, A. S.; Zalessky, A. V.; Bush, A. A.; Baenitz, M.; Rosner, H.; Drechsler, S.-L. *Phys. Rev. B* **2004**, *70*, 020406(R).
(8) Masuda, T.; Zheludev, A.; Bush, A.; Markina, M.; Vasiliev, A. *Phys. Rev. Lett.* **2004**, *92*, 177201.
(9) Chen, M.; Hu, C. D. *J. Phys. Soc. Jpn.* **2014**, *83*, 014702.
(10) Rumbold, B. D.; Wilson, G. V. H. *J. Phys. Chem. Solids* **1974**, *35*, 241−248.
(11) Hanzel, D.; Tressaud, A.; Dance, J.-M.; Hagenmuller, P. *Solid State Commun.* **1977**, *22*, 215−218.
(12) Niesen, S. K.; Heyer, O.; Lorenz, T. T.; Valldor, M. *J. Magn. Magn. Mater.* **2011**, *323*, 2575−2578.
(13) Mole, R. A.; Stride, J. A.; Unruh, T.; Wood, P. T. *J. Phys.: Condens. Matter* **2009**, *21*, 076003.
(14) (a) Garlea, V. O.; Sanjeewa, L. D.; McGuire, M. A.; Kumar, P.; Sulejmanovic, D.; H, J.; Hwu, S.-J. *Phys. Rev. B* **2014**, *89*, 014426. (b) Choi, K.-Y.; Choi, I. H.; Lemmens, P.; van Tol, J.; Berger, H. *J. Phys.: Condens. Matter* **2014**, *26*, 086001. (c) Sun, L.-Z.; Sun, W.; Ren, W.-J.; Zhang, J.-Y.; Huang, Y.-X.; Sun, Z.-M.; Pan, Y.; Mi, J.-X. *J. Solid State Chem.* **2014**, *212*, 48−57. (d) Machens, A.; Konstantinidis, N. P.; Waldmann, O.; Schneider, I.; Eggert, S. *Phys. Rev. B* **2013**, *87*, 144409.
(15) (a) *Functional Oxides*; Bruce, D. W., O'Hare, D., Walton, R. I., Eds.; Wiley: Chichester, U.K., 2010; Chapters 1 and 2. (b) Mao, J.-G.; Jiang, H.-L.; Kong, F. *Inorg. Chem.* **2008**, *47*, 8498−8510.
(16) (a) Janson, O.; Tsirlin, A. A.; Osipova, E. S.; Berdonosov, P. S.; Olenev, A. V.; Dolgikh, V. A.; Rosner, H. *Phys. Rev. B* **2011**, *83*, 144423. (b) Becker, R.; Prester, M.; Berger, H.; Lin, P. H.; Johnsson, M.; Drobac, D.; Zivkovic, I. *J. Solid State Chem.* **2007**, *180*, 1051−1059. (c) Becker, R.; Johnsson, M.; Kremer, R. K.; Lemmens, P. *J. Solid State Chem.* **2005**, *178*, 2024−2029. (d) Becker, R.; Berger, H.; Johnsson, M.; Prester, M.; Marohnic, Z.; Miljak, M.; Herak, M. *J. Solid State Chem.* **2006**, *179*, 836−842. (e) Becker, R.; Prester, M.; Berger, H.; Johnsson, M.; Drobac, D.; Zivkovic, I. *Solid State Sci.* **2007**, *9*, 223−230. (f) Becker, R.; Johnsson, M.; Berger, H.; Prester, M.; Zivkovic, I.; Drobac, D.; Miljak, M.; Herak, M. *Solid State Sci.* **2006**, *8*, 836−842. (g) Johnsson, M.; Törnroos, K. W.; Mila, F.; Millet, P. *Chem. Mater.* **2000**, *12*, 2853−2857. (h) Baek, S.-H.; Choi, K.-Y.; Berger, H.; Büchner, B.; Grafe, H.-J. *Phys. Rev. B* **2012**, *86*, 180405(R). (i) Uematsu, D.; Sato, M. *J. Phys. Soc. Jpn.* **2007**, *76*, 084712. (j) Johnsson, M.; Törnroos, K. W.; Lemmens, P.; Millet, P. *Chem. Mater.* **2003**, *15*, 68−73. (k) Jiang, H.-L.; Mao, J.-G. *Inorg. Chem.* **2006**, *45*, 7593−7599. (l) Johnsson, M.; Lidin, S.; Törnroos, K. W.; Bürgi, H.-B.; Millet, P. *Angew. Chem., Int. Ed.* **2004**, *43*, 4291−4295. (m) Zhang, D.; Johnsson, M.; Lidin, S.; Kremer, R. K. *Dalton Trans.* **2013**, *42*, 1394−1399.
(17) Zimmermann, I.; Kremer, R. K.; Reuvekamp, P.; Johnsson, M. *Dalton Trans.* **2013**, *42*, 8815−8819.
(18) Hu, S.; Johnsson, M. *Dalton Trans.* **2013**, *42*, 7859−7862.
(19) (a) Zhang, D.; Johnsson, M.; Berger, H.; Kremer, R. K.; Wulferding, D.; Lemmens, P. *Inorg. Chem.* **2009**, *48*, 6599−6603. (b) Becker, R.; Johnsson, M. *J. Solid State Chem.* **2007**, *180*, 1750−1758. (c) Becker, R.; Johnsson, M.; Kremer, R. K.; Klauss, H.-H.; Lemmens, P. *J. Am. Chem. Soc.* **2006**, *128*, 15469−15475. (d) Zhang, D.; Kremer, R. K.; Lemmens, P.; Choi, K.-Y.; Liu, J.; Whangbo, M.-H.; Berger, H.; Skourski, Y.; Johnsson, M. *Inorg. Chem.* **2011**, *50*, 12877−

12885. (e) Hu, S.; Johnsson, M.; Law, J. M.; Bettis, J. L., Jr.; Whangbo, M.-H.; Kremer, R. K. *Inorg. Chem.* **2014**, *53*, 4250−4256.
(20) Kauzlarich, S. M.; Stanton, J. L.; Faber, J.; Averill, B. A. *J. Am. Chem. Soc.* **1986**, *108*, 7946−7951.
(21) *SMART and SAINT*; Bruker AXS, Madison, WI, USA, 2007.
(22) Sheldrick, G. M. *SADABS*; University of Göttingen, Göttingen, Germany, 1996.
(23) Sheldrick, G. M. *Acta Crystallogr., Sect. A* **2008**, *A64*, 112−122.
(24) Matsnev, M. E.; Rusakov, V. S. *AIP Conf. Proc.* **2012**, *1489*, 178−185.
(25) (a) Kresse, G.; Hafner, J. *Phys. Rev. B* **1993**, *47*, R558. (b) Kresse, G.; Furthműller, J. *Phys. Rev. B* **1996**, *54*, 11169.
(26) Perdew, J. P.; Burke, K.; Ernzerhof, M. *Phys. Rev. Lett.* **1996**, *77*, 3865−3868.
(27) Brese, N. E.; O'Keeffe, M. *Acta Crystallogr.* **1991**, *B47*, 192−197.
(28) Brown, I. D. http://www.iucr.org/__data/assets/file/0006/81087/bvparm2013.cif.
(29) (a) Zvereva, E. A.; Savelieva, O. A.; Primenko, A. E.; Ibragimov, S. A.; Slyn'ko, E. I.; Slyn'ko, V. E. *J. Appl. Phys.* **2010**, *108*, 093923. (b) Battles, J. W. *J. Appl. Phys.* **1971**, *42*, 1286−1287. (c) Oseroff, S.; Calvo, R.; Giriat, W. *J. Appl. Phys.* **1979**, *50*, 7738−7739. (d) Zvereva, E. A.; Evstigneeva, M. A.; Nalbandyan, V. B.; Savelieva, O. A.; Ibragimov, S. A.; Volkova, O. S.; Medvedeva, L. I.; Vasiliev, A. N.; Klingeler, R.; Büchner, B. *Dalton Trans.* **2012**, *41*, 572−580. (e) Wolter, A. U. B.; Lipps, F.; Schäpers, M.; Drechsler, S.-L.; Nishimoto, S.; Vogel, R.; Kataev, V.; Büchner, B.; Rosner, H.; Schmitt, M.; Uhlarz, M.; Skourski, Y.; Wosnitza, J.; Süllow, S.; Rule, K. C. *Phys. Rev. B* **2012**, *85*, 014407. (f) Elliston, P. R. *J. Phys. C: Solid State Phys.* **1974**, *7*, 425−429.
(30) (a) Kufuata, J.; Sadłwski, L.; Bojanowski, B.; Walczak, J.; Kurzawa, M.; Pichet, J. *Phys. Status Solidi A* **1988**, *109*, K139−K143. (b) Walczak, J.; Kurzawa, M.; Kuiuata, J.; Sadłowski, L. *Phys. Status Solidi B* **1985**, *132*, K99−K102. (c) Guskos, N.; Likodimos, V.; Glenis, S.; Patapis, S. K.; Palilis, L. C.; Typek, J.; Wabia, M.; Rychlowska-Himmel, I. *Phys. Rev. B* **1999**, *60*, 7687−7690. (d) Zvereva, E. A.; Savelieva, O. A.; Titov, Y. D.; Evstigneeva, M. A.; Nalbandyan, V. B.; Kao, C. N.; Lin, J.-Y.; Presniakov, I. A.; Sobolev, A. V.; Ibragimov, S. A.; Abdel-Hafiez, M.; Krupskaya, Yu.; Jähne, C.; Tan, G.; Klingeler, R.; Buechner, B.; Vasiliev, A. N. *Dalton Trans.* **2013**, *42*, 1550−1566. (e) Causa, M. T.; Tovar, M.; Obradors, X.; Labarta, A.; Tejada, J. *Phys. Rev. B* **1991**, *44*, 4455−4460.
(31) Huber, D. L. *Phys. Rev. B* **1972**, *6*, 3180−3186.
(32) (a) Kawasaki, K. *Prog. Theor. Phys.* **1968**, *39*, 285−311. (b) Kawasaki, K. *Phys. Lett. A* **1968**, *26*, 543.
(33) Mori, H.; Kawasaki, K. *Prog. Theor. Phys.* **1962**, *28*, 971−987.
(34) Webb, D. J.; Bhagat, S. M.; Furdyna, J. K. *J. Appl. Phys.* **1984**, *55*, 2310−2312.
(35) Richards, P. M. *Solid State Commun.* **1973**, *13*, 253−255.
(36) Andres, A. G.; Volotski, S. V. *J. Magn. Magn. Mater.* **1983**, *31*−*34*, 1169−1170.
(37) Kaul, E. E.; Rosner, H.; Yushankhai, V.; Sichelschmidt, J.; Shpanchenko, R. V.; Geibel, C. *Phys. Rev. B* **2003**, *67*, 174417.
(38) Goodenough, J. B. *Magnetism and the chemical bond*; Wiley: New York, 1976.
(39) Fisher, M. *Am. J. Phys.* **1964**, *32*, 343.
(40) Bain, G. A.; Berry, J. F. *J. Chem. Educ.* **2008**, *85*, 532−536.
(41) Oguchi, T. *Phys. Rev.* **1964**, *A133*, 1098.
(42) Menil, F. *J. Phys. Chem. Solids* **1985**, *46*, 763−789.
(43) Van der Woude, F.; Sawatzky, G. A. *Phys. Rev. B* **1971**, *4*, 3159−3164.
(44) Gupta, G. P.; Dickson, D. P. E.; Johnson, C. E. *J. Phys. C: Solid State Phys.* **1978**, *11*, 215−225.
(45) Andersen, O. K.; Saha-Dasgupta, T. *Phys. Rev. B* **2000**, *62*, 16219(R).
(46) Kugel, K. I.; Khomskii, D. I. *Sov. Phys. Usp.* **1982**, *25*, 231−256.
(47) (a) Valentí, R.; Saha-Dasgupta, T.; Alvarez, J. V.; Požgajčić, K.; Gros, C. *Phys. Rev. Lett.* **2001**, *86*, 5381−5384. (b) Saha-Dasgupta, T.; Valentí, R.; Capraro, F.; Gros, C. *Phys. Rev. Lett.* **2005**, *95*, 107201. (c) Das, H.; Saha-Dasgupta, T.; Gros, C.; Valentí, R. *Phys. Rev. B* **2008**, *77*, 224437. (d) Pregelj, M.; Jeschke, H. O.; Feldner, H.; Valentí, R.; Honecker, A.; Saha-Dasgupta, T.; Das, H.; Yoshii, S.; Morioka, T.; Nojiri, H.; Berger, H.; Zorko, A.; Zaharko, O.; Arčon, D. *Phys. Rev. B* **2012**, *86*, 054402. (e) Reehuis, M.; Saha-Dasgupta, T.; Orosel, D.; Nuss, J.; Rahaman, B.; Keimer, B.; Andersen, O. K.; Jansen, M. *Phys. Rev. B* **2012**, *85*, 115118.
(48) Drechsler, S.-L.; Richter, J.; Kuzian, R.; Malek, J.; Tristan, N.; Büchner, B.; Moskvin, A. S.; Gippius, A. A.; Vasiliev, A.; Volkova, O.; Prokofiev, A.; Rakoto, H.; Broto, J.-M.; Schnelle, W.; Schmitt, M.; Ormeci, A.; Loison, C.; Rosner, H. *J. Magn. Magn. Mater.* **2007**, *316*, 306−312.
(49) Vasil'ev, A. N.; Pryadun, V. V.; Khomskii, D. I.; Dhalenne, G.; Revcolevschi, A.; Isobe, M.; Ueda, Y. *Phys. Rev. Lett.* **1998**, *81*, 1949−1952.
(50) Sologubenko, A. V.; Gianno, K.; Ott, H. R.; Vietkine, A.; Revcolevschi, A. *Phys. Rev. B* **2001**, *64*, 054412.
(51) Sun, X. F.; Liu, X. G.; Chen, L. M.; Zhao, Z. Y.; Zhao, X. *J. Appl. Phys.* **2013**, *113*, 17B514.
(52) Hess, C.; Baumann, C.; Ammerahl, U.; Buchner, B.; Heidrich-Meisner, F.; Brenig, W.; Revcolevschi, A. *Phys. Rev. B* **2001**, *64*, 184305.
(53) Shlagman, O.; Shimshoni, E. *Phys. Rev. B* **2012**, *86*, 075442.